PERGAMON

Journal of Structural Geology 25 (2003) 855–866

JOURNAL OF STRUCTURAL GEOLOGY

www.elsevier.com/locate/jsg

Grain size stabilisation by dispersed graphite in a high-grade quartz mylonite: an example from Naxos (Greece)

Maarten Krabbendam[a,*], Janos L. Urai[b], Lucas J. van Vliet[c]

[a]*British Geological Survey, Murchison House, West Mains Road, Edinburgh EH9 3LA, UK*
[b]*Geologie-Endogene Dynamik, Aachen University of Technology RWTH, Lochnerstrasse 4-20, D-52056 Aachen, Germany*
[c]*Pattern Recognition Group of the Faculty of Applied Sciences, Delft University of Technology, Lorentzweg 1, 2628 CJ Delft, The Netherlands*

Received 1 December 2001; received in revised form 21 June 2002; accepted 27 June 2002

Abstract

High grade quartz mylonites from Naxos, Greece, consist of alternating thin layers of pure quartz and quartz layers with 0.3–3 vol.% finely dispersed graphite particles. Graphite-free layers are coarse grained (100–300 μm), show undulose extinction, subgrains, lobate grain boundaries and have a strongly developed crystallographic preferred orientation. In these layers, dislocation flow is interpreted to be the dominant deformation mechanism. In contrast, graphite-rich layers are fine-grained (30–70 μm), have equant quartz grain shapes and have a crystallographic preferred orientation that becomes progressively weaker with decreasing quartz grain size. Given the high temperature of deformation and the need for a *c*-axis fabric destroying mechanism, grain boundary sliding is interpreted to be important in these layers. Analysis shows an inverse relationship between quartz grain size and the graphite dispersion, suggesting stabilization of quartz grain size by graphite particles. Graphite particles larger than 5 μm are concentrated along quartz boundaries, suggesting that stabilisation only operates above a certain critical graphite particle size. This study shows that a dispersed second phase such as graphite in a naturally deforming rock can inhibit grain boundary migration, stabilise the grain size and enhance grain boundary sliding at the expense of dislocation flow.

Keywords: Graphite particles; Quartz mylonite; Crystallographic preferred orientation; Grain boundary sliding

1. Introduction

Ductile deformation of rocks by dislocation flow usually results in a change of grain size. The dominant process for grain size reduction is dynamic recrystallization where grain boundary migration, sub-grain rotation and the formation of new grains can all operate simultaneously (e.g. Schmid, 1982; Urai et al., 1986; Humphreys and Hatherly, 1996). During dynamic recrystallisation, grain growth and grain size reduction compete with each other and under steady state deformation this results in a grain size that is in dynamic equilibrium with the operating deviatoric stress (e.g. Twiss, 1977; de Bresser et al., 1998).

Finely dispersed second phase particles may inhibit grain growth and stabilise the grain size well below the steady state recrystallised grain size. A finely dispersed second phase may thus cause a switch from grain-size insensitive dislocation flow to grain size sensitive deformation mechanisms such as grain boundary sliding or diffusion creep (Etheridge and Wilkie, 1979; Olgaard, 1990). In this manner a second phase can strongly affect the rheology of rocks and, if second phase particles are heterogeneously distributed, strain localisation may occur. During recrystallisation, migrating grain boundaries can have three basic types of interaction with solid second phases (Fig. 1; Drury and Urai, 1990; Urai and Jessell, 2001).

1. Grain boundaries can migrate relatively unaffected by an immobile second phase when the driving force for the grain boundary migration is larger than the dragging force exerted by second phase particles.
2. The grain boundaries can be pinned by immobile particles, resulting in cessation of grain growth and stabilisation of grain size (Olgaard and Evans, 1986) when the driving force for grain boundary migration is smaller than the dragging force of second phase particles.

* Corresponding author. Tel.: +44-131-667-1000; fax: +44-131-6500-256.
E-mail addresses: mkrab@bgs.ac.uk (M. Krabbendam), j.urai@ged.rwth-aachen.de (J.L. Urai), L.J.vanVliet@ph.tn.tudelft.nl (L.J. van Vliet).

0191-8141/03/$ - see front matter © 2002 Elsevier Science Ltd. All rights reserved.
PII: S0191-8141(02)00086-X

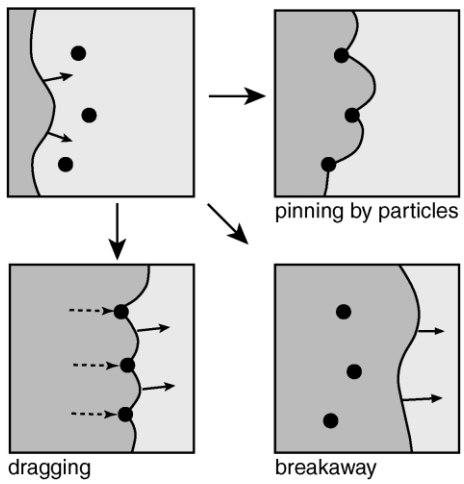

Fig. 1. Schematic diagram illustrating the possible interactions of second phase particles and a migrating grain boundary. See text for discussion (after Drury and Urai, 1990).

3. Grain boundaries may drag the particles through the matrix when the second phase is sufficiently mobile to move through the material (Ashby and Centramore, 1968). In turn, second phase may evolve also during the process (Herwegh and Jenni, 2001) resulting in complex feedback processes that may be much more common in metamorphic rocks than recognized to date.

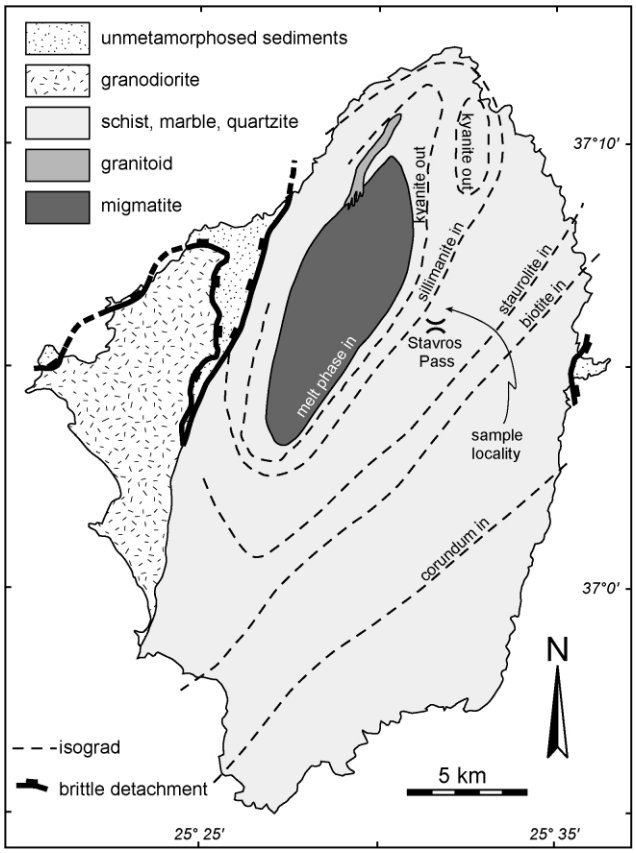

Fig. 2. Simplified geological map of Naxos, Greece, showing rock types and metamorphic isograds (after Jansen and Schuiling, 1976; Kreulen, 1977; Lister et al., 1984; Urai et al., 1990). The samples analysed in this study are all from the vicinity of Stavros Pass.

The second type of interaction has the greatest influence on grain size and hence on rheology. In the absence of deformation the relation between the stabilised grain size D_{max} and the dispersion of the second phase particles is described by equations of the type:

$$D_{max} = C\frac{d}{f^m} \text{ or } \log D_{max} = \log d - m\log f \quad (1)$$

where C is a constant, d is the effective diameter of the second phase particles, f is the volume fraction of the second phase and m is a parameter to describe the geometry of the dispersion. When all the particles are randomly distributed through the material, $m = 1$, when the particles are concentrated along grain boundaries, $m = 1/2$, and in the case of concentration along triple junctions, $m = 1/3$ (Olgaard and Evans, 1986, 1988; Evans et al., 2001). The right hand side of the equation is an inverse measure of dispersion.

In this paper we aim to answer the following questions: has second phase pinning occurred in quartzite samples deformed under amphibolite facies conditions and is Eq. (1) a valid representation of the microstructural evolution? Did second phase pinning result in grain size stabilisation below the steady-state dislocation flow grain size and did this, in turn, result in a change in deformation mechanism from dislocation flow to grain boundary sliding in quartz? To answer these questions, we present and discuss crystallographic preferred orientation (CPO), quartz grain size, second phase particle dispersion and other microstructural data from naturally deformed graphitic quartz mylonites from Naxos, Greece.

2. Geological setting

The geology of Naxos (Fig. 2) is dominated by an Alpine metamorphic core complex (Lister et al., 1984; Urai et al., 1990). Naxos consists of a migmatitic gneiss core with Hercynian protolith, overlain by a package of high-grade Mesozoic metasediments, in turn overlain by non-metamorphosed rocks of mainly Miocene age. The metamorphic rocks have undergone an Eocene (~45 Ma; Andriessen et al., 1979) high-pressure, low-temperature tectono-metamorphic event, M1 (Avigad, 1998), followed by an Early Miocene (20–16 Ma; Wijbrans and McDougall, 1988) high-temperature, low-pressure metamorphism (M2) with conditions ranging from $T \sim 400$ °C and $P \sim 4$–5 kbar in the south to $T \sim 700$ °C and $P \sim 6$–7 kbar in the migmatitic core (Jansen and Schuiling, 1976; Buick and Holland, 1989; Urai and Feenstra, 2001). The M2 event produced the current closely spaced isograds and the migmatitic core. M2 was coeval with and caused by a north–south extensional

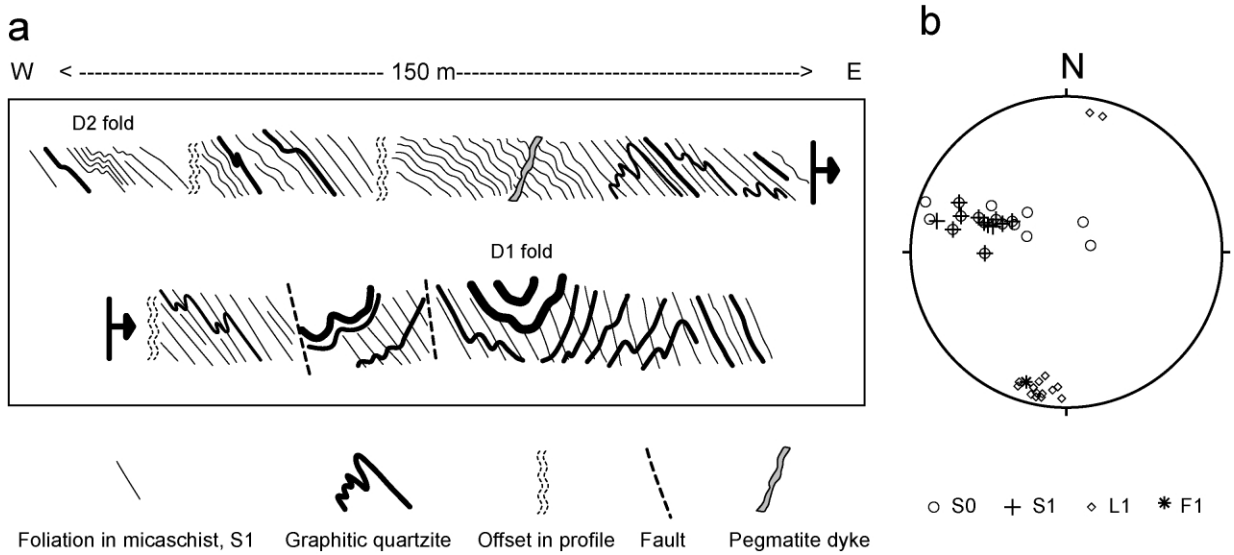

Fig. 3. (a) Schematic profile of road cut north of Stavros Pass, showing tightly to isoclinally folded graphitic quartzite layers embedded in mica schist. Plane of profile is at high angle to stretching lineation. Crenulation of the dominant foliation in the schists due to D2, D3 and late faulting (Urai et al., 1990) are not discussed further in this paper. (b) Stereoplot of main structural data from this profile. Equal area lower hemisphere projection.

deformational phase with a strong top-to-the-north non-coaxial shearing component, focused in Naxos at mid-crustal levels (Lister et al., 1984; Buick and Holland, 1989; Urai et al., 1990; Buick, 1991; Urai and Feenstra, 2001). In common with other metamorphic core complexes, the close spacing of the isograds was caused by a combination of high geothermal gradient instigated by the extensional event and by attenuation of the isograds during that same extensional event. The syn-M2 extensional deformation phase produced the mylonites that are the subject of this study. Locally, sheath folds developed in this mid-crustal shear zone (Urai et al., 1990). A later phase of deformation during further exhumation and cooling was associated with the overlying brittle extensional detachment and final exhumation of the metamorphic core complex and produced narrow post-peak M2 mylonites (Lister et al., 1984; Urai et al., 1990).

The quartz mylonites investigated in this study were sampled near Stavros Pass, close to the sillimanite isograd and only a short distance from the migmatitic core (Fig. 2). The samples form part of the main syn-M2 mid-crustal shear zone and were deformed at temperatures between 500 and 650 °C (see also Urai et al., 1990; Buick, 1991). Samples affected by the narrow, strongly localized post-peak-M2 shear zones that developed during uplift and cooling (e.g. Urai et al., 1990) were excluded from this study.

Fig. 4. Photograph of a typical tightly folded quartzite in mica schist showing strongly developed stretching lineation parallel to the fold axes. Stavros Pass road cut. View to NW, width of view about 2 m.

3. Meso- and microstructures

In outcrop, graphitic quartzite (containing quartz, minor graphite and accessory mica) is intercalated with mica schist, in layers 5–50 cm thick. These rocks contain a well-developed mylonitic foliation and tight to isoclinal folds with fold axes that are parallel to the strongly developed N–S stretching lineation (Figs. 3 and 4). The foliation in the quartzite is defined by alternating millimetre-sized graphite-rich layers and graphite-free layers (Fig. 5a). This mylonitic foliation in the quartzite is probably strongly modified bedding, which is isoclinally folded without the development of an axial planar foliation. In contrast, the foliation in the mica schist is axial planar to the isoclinal folds in the quartzites (Fig. 3).

The samples studied in this project were taken from the limbs of tight to isoclinal folds, where the mylonitic foliation of the quartzite is subparallel to the foliation in the mica schist. Thin sections of quartzites were cut normal to the foliation and parallel to the lineation. In thin section, all samples show comparable microstructures so that the descriptions presented below apply to all samples.

The microstructure of the graphite-free layers is

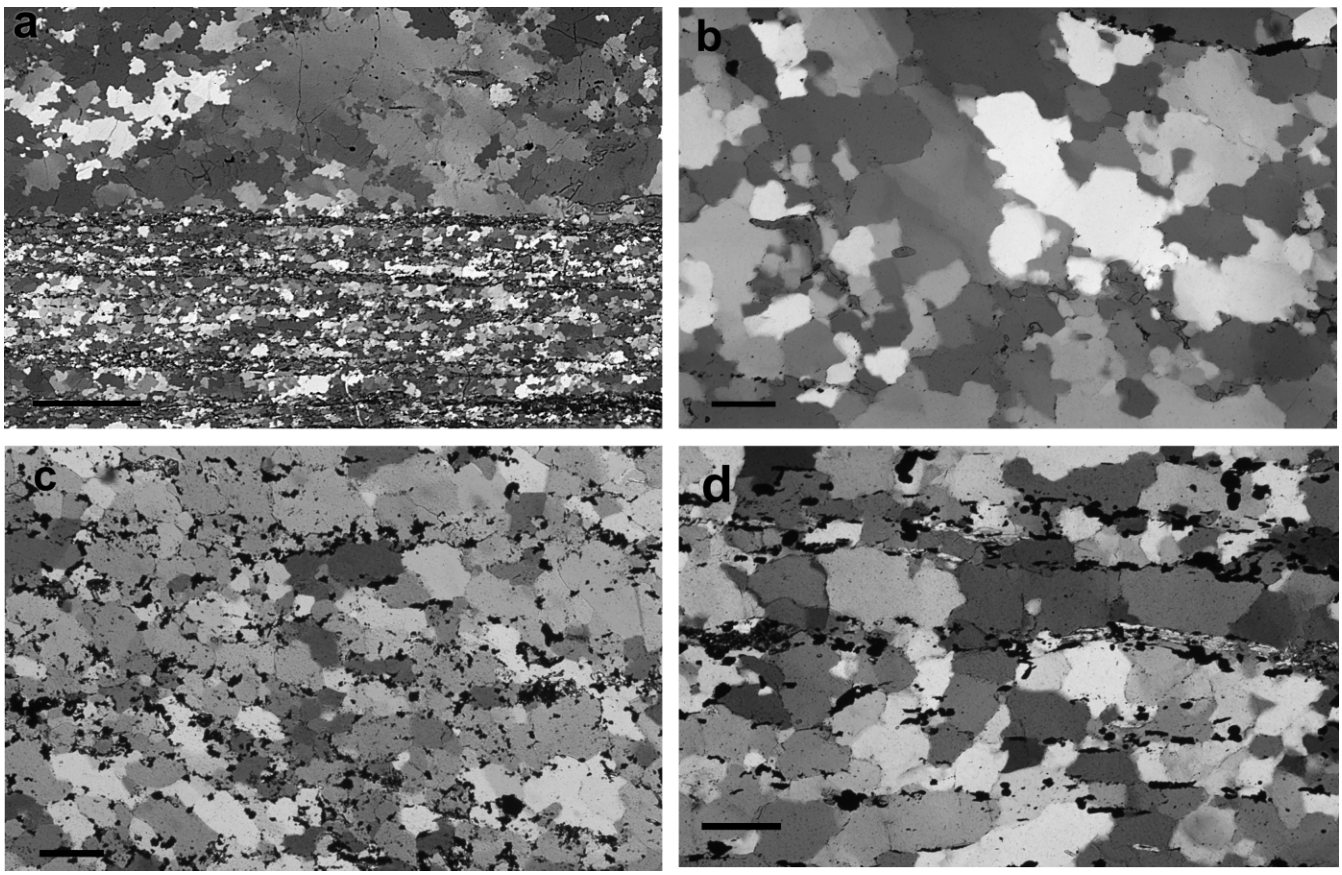

Fig. 5. Microphotographs of graphitic quartzite mylonites. (a) Graphite-rich quartzite. Coarse grained, graphite-free layers and fine-grained, graphite-rich layers form a mylonitic foliation. Scale bar is 1 mm. Sample 4, top half is layer 4.1; bottom half is layer 4.2. Numbering (e.g. 4.1) refers to sample 4 and layer 1 in this thin section. XPL and gypsum plate. (b) Graphite-free layer. Lobate grain boundaries, subgrains and triple junctions are visible. Scale bar is 0.1 mm. Sample 8, layer 8.1. XPL and gypsum plate. (c) Fine-grained graphite-rich layer. Domains with the most dispersed graphite have the smallest grain size. Graphite particles tend to concentrate along grain boundaries and triple junctions, although very small graphite particles also occur within the quartz grains. Subgrains and lobate grain boundaries only occur in small graphite-free domains. Scale bar is 0.1 mm. Sample 8, layer 8.3. Partially crossed nicols and gypsum plate. (d) Quartz layer just above centre is bounded by two thin, continuous layers of graphite and mica particles. The quartz grains form a ribbon elongated parallel to the graphite layers. Scale bar is 0.1 mm. Sample 5; XPL and gypsum plate.

characterised by a coarse grain size ($D_{qtz} \sim 100–300$ μm), undulose extinction, sub-grains and lobate grain boundaries (Fig. 5b). These microstructures are common in dynamically recrystallised quartz at high temperatures (Tullis et al., 1973; White et al., 1980; Urai et al., 1986).

In comparison with the graphite-free layers, the grain size in the graphite-rich layers is smaller ($D_{qtz} \leq 30–70$ μm). The quartz microstructure in the graphite-rich layers contains less obvious evidence of dynamic recrystallisation. In quartz domains between graphite particles, weak undulose extinction and lobate grain boundaries occur. In layers or domains with very fine grain size ($D_{qtz} < 50$ μm) and a high dispersion of graphite, quartz has a near-equant grain shape and does not show undulose extinction, subgrains or lobate grain boundaries (Figs. 5c and 6b).

Graphite particle size ranges from less than 5 μm to about 40 μm (Fig. 7). Small graphite particles ($d_{graph} < 5$ μm) occur as inclusions within the quartz grains, whereas graphite particles with $d_{graph} > 5–10$ μm tend to concentrate along quartz grain boundaries and triple junctions (Fig. 6b). Long graphite trails also occur, with elongate graphite aggregates, commonly forming the boundaries between graphite-rich and graphite-free layers. Locally, quartz ribbons occur, bounded by thin, near-continuous graphite layers (Fig. 5d).

4. Dispersion of graphite particles and quartz grain size

4.1. Methods

The quartz grain size D_{qtz} and the dispersion of the graphite particles were determined in several domains in one thin section (Sample 8). The quartz grain size of the different domains was measured using the linear intercept method.

To determine the degree of dispersion (and values of the parameters d and f in Eq. (1)), microphotographs of selected domains of the thin section were captured with a microscope-mounted video camera, using plain polarised light. All domains measured 0.6×0.6 mm and contained

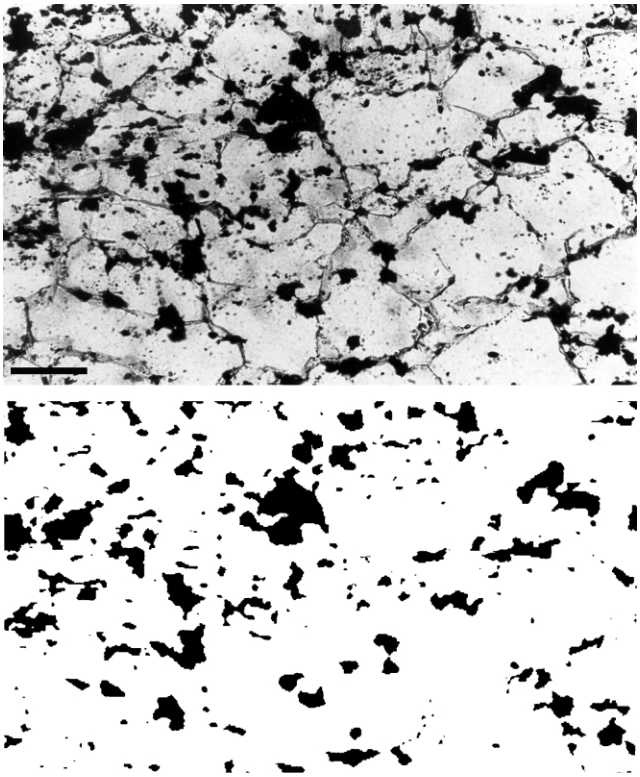

Fig. 6. Segmented binary image (bottom) compared with PPL microphotograph of the same area (top). Graphite particles with the smallest diameter (~5 μm) occur within the quartz grains. Larger graphite particles are concentrated along grain boundaries and triple junctions. See text for discussion. Scale bar is 0.1 mm, Sample 8.

100–400 graphite particles. The greyscale images were digitally reprocessed to produce a binary (black and white) image. The contrast, cut off value, light intensity, microscope diaphragm and several filters were adjusted manually to give a result as close to the original as possible (Fig. 6). From the binary image, the graphite volume fraction f and the average area a of the graphite particles were calculated. Only the average area of grains entirely positioned within the image was calculated. We used the square root of the average area ($\sqrt{a}$) as an approximation of the effective particle diameter d. The graphite area fraction was used to calculate the graphite volume fraction, correcting for the bias due to the finite thickness of the thin section (see Appendix 1 for details of the method).

4.2. Results

In the different layers analysed in Sample 8, quartz grain size varies between 38 and 63 μm; the graphite volume fraction f varies from 0.003 to 0.03, whereas the average graphite particle diameter d_{graph} varies from 7 to 16 μm. Despite some scatter, a clear inverse relationship between the quartz grain size D_{qtz} and the graphite volume fraction f exists (Fig. 7a). No clear relationship is obvious between D_{qtz} and d_{graph} (Fig. 7b). This may be because the range of d is much smaller (between 7 and 16 μm) than the range in

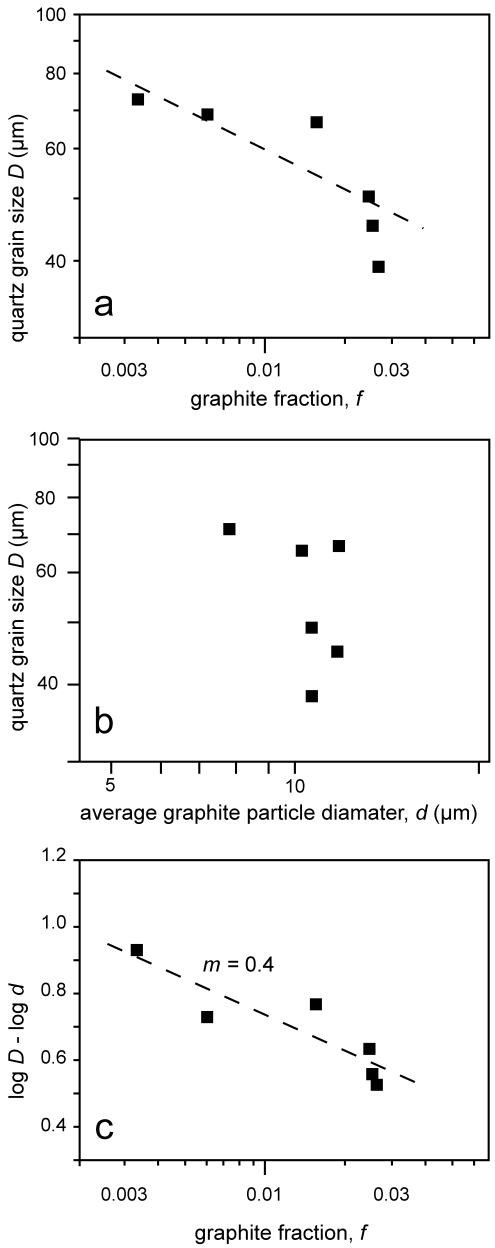

Fig. 7. (a) Logarithmic plot of quartz grain size D against graphite fraction f, with linear fit. Each point represents measurements of one domain. (b) Logarithmic plot of quartz grain size D against average graphite particle diameter d, showing absence of a correlation. (c) Logarithm of quartz grain size divided by average graphite particle diameter d ($\log D - \log d$ in μm) plotted against the graphite fraction ($\log f$), with linear fit. Factor m is about 0.4.

diameter of individual graphite particles (ranging from <5 to >40 μm). Also, the range of d_{graph} is small compared with the range of f. The quartz grain size D_{qtz} appears thus to be mainly controlled by the graphite volume fraction f, and to a lesser degree by the average particle diameter.

To compare our data with Eq. (1), we plotted $\log D_{qtz} - \log d_{graph}$ against $\log f$. The slope of this graph (Fig. 7c) can now be compared with the factor m, with a value of around 0.40, which is consistent with the observation that graphite

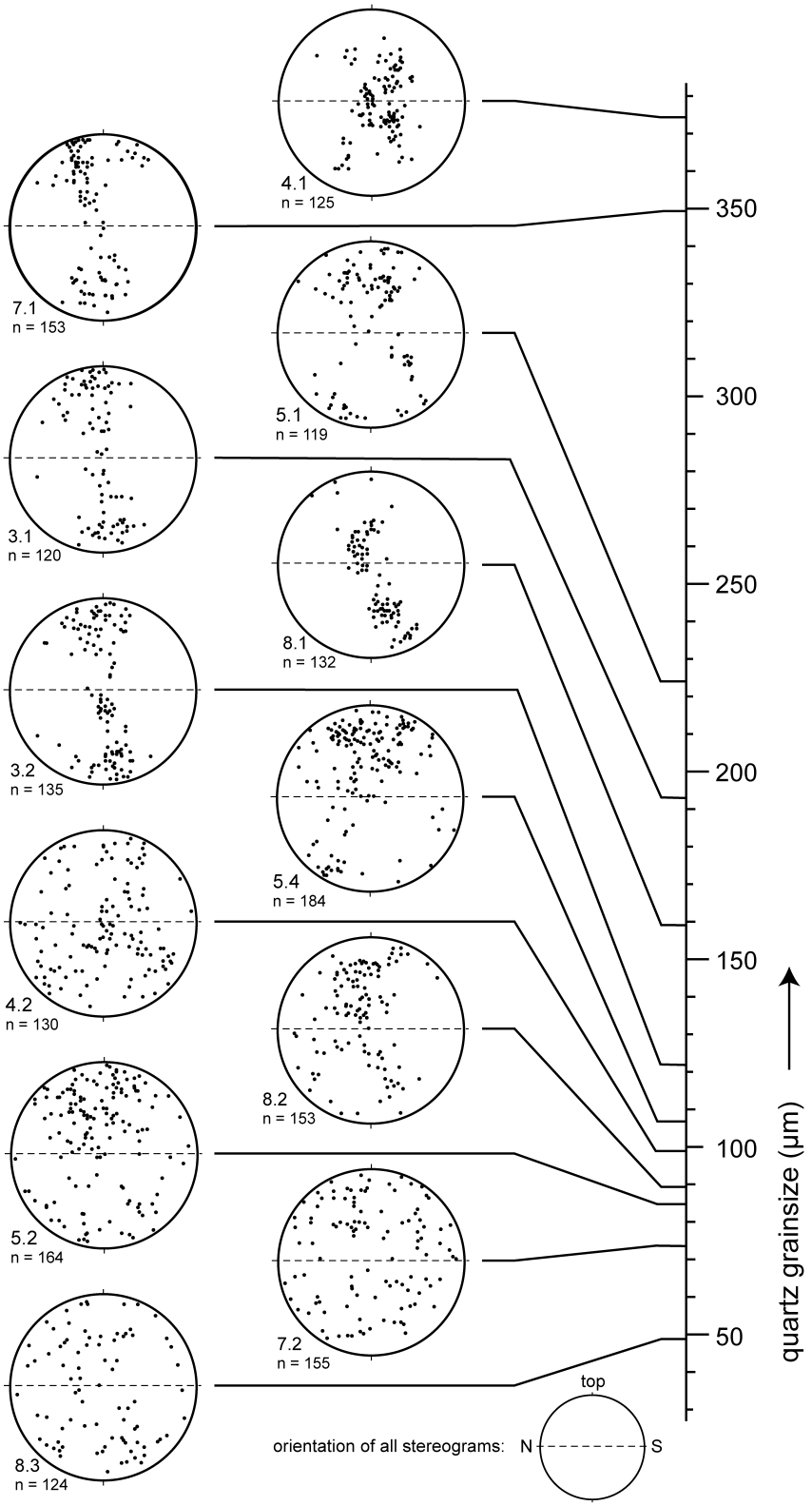

Fig. 8. *c*-Axis fabrics of samples 3–5, 7 and 8. From each sample different layers were analysed (3.1, 3.2, etc.), which are plotted against the quartz grain size of each layer. Equal area, upper hemisphere projection. Sample orientation shown at bottom of figure.

particles are concentrated along grain boundaries and triple junctions (Olgaard and Evans, 1986, 1988).

5. Crystallographic preferred orientation (CPO), methods and results

Quartz *c*-axes were measured in five samples on an automatic U-stage (developed by G.S. Lister at Utrecht University) and with a conventional U-stage in the case of fine-grained layers. Two to three layers with different grain size and graphite dispersion were measured in each sample.

In Fig. 8, fabrics from different layers in different samples are plotted against the quartz grain size of the particular layer. The graphite-free layers with a quartz grain size larger than 150 μm show a well-developed CPO of girdles or point maxima, consistent with the strong non-coaxiality of the regional deformation (e.g. Urai et al., 1990). Graphite-rich layers with a grain size between 70 and 150 μm have weakly developed CPO fabrics. The fabrics are not totally random; certain pole-free areas still occur, but girdles or point maxima are not clearly defined. Layers with the smallest quartz grain sizes ($D_{qtz} = 50$ to 70 μm) show no significant pattern in the *c*-axis orientations. Thus, below a grain size of approximately 100 μm, CPO development becomes progressively weaker with decreasing grain size, tending towards random orientations at the smallest grain size. These changes are seen in all thin sections that contain layers with sufficiently high graphite content.

In summary, the graphite-free layers have a coarse grain size, a well developed CPO and microstructures typical for dynamic recrystallisation. The graphite-rich layers have a fine grain size, a poorly to non-developed CPO and only rarely microstructures that are typical for dynamic recrystallisation. We interpret the significant weakening of the CPO and the weakening of the developed recrystallised microstructures to be associated with a decreasing grain size and an increasing dispersion of the graphite particles.

In layers that do posses a distinct *c*-axis fabric, there is quite a variety in *c*-axis girdle patterns, e.g. asymmetric Type I and Type II crossed girdles and point maxima. It is unlikely that these variations are the result of different temperatures of deformation (e.g. Passchier and Trouw, 1996; Takeshita, 1996), since it is likely that the samples were deformed under very similar *P* and *T* conditions. Rather, the variations can probably best be explained by heterogeneous strain, such as local variations of the vorticity number, deviations from plane strain and absolute variations of the finite strain (Law, 1990).

6. Discussion

6.1. Second phase pinning and stabilisation of grain size

The relationship between stabilised grain size and particle dispersion (Eq. (1)) is well known for metals and ceramics. To date, it has only been studied in minerals during static recrystallisation experiments on marble with fine mica as the second phase (Olgaard and Evans, 1988). One important question is whether Eq. (1) is also generally valid during deformation and dynamic recrystallisation. Our data suggest that such a relationship can also exist in deforming rocks, as long as *D* is kept sufficiently small to suppress dislocation creep in the grains.

From Eq. (1) it follows that, at a constant volume fraction of particles *f*, a decreasing particle diameter *d* (i.e. a finer dispersion) would result in a decreasing stabilised quartz grain size, D_{qtz}. In other words, few *large* particles are not able to control the grain size throughout the rock. On the other hand, to inhibit grain boundary migration *locally,* the dragging force of a single particle should be equal to or greater than the *local* grain boundary driving force. The maximum dragging force per particle is proportional to its diameter (Stüwe, 1978), so that *small* particles also are ineffective in pinning grain boundaries.

Let us now consider the following aspects:

1. The factor *m* in formula (1) implies that grain boundary pinning is much more effective if particles are concentrated along grain boundaries and triple junctions ($m = 0.5–0.3$) rather than uniformly distributed ($m = 1$) and particles are also located within the grains.
2. In our samples, small graphite particles ($d_{graph} < 5$ μm) commonly occur within quartz grains whereas larger particles ($d_{graph} > 5–10$ μm) are concentrated along grain boundaries and triple junctions (Fig. 7).

We suggest therefore that a minimum diameter of second phase particles is required to pin grain boundaries effectively and that Eq. (1) is valid only above this critical minimum value. In the case of high temperature deformation of the graphitic mylonites this minimum particle diameter appears to be in the order of 5 μm.

6.2. Deformation mechanisms

The observed microstructures (undulose extinction, subgrains, lobate grain boundaries) and the strong CPO in the graphite-free layers, strongly suggest that the dominant deformation in these layers was dislocation flow resulting in dynamic recrystallisation (see also Buick, 1991). The deformation mechanism that was dominant in the graphite-rich layers is less clear. The absence of a well developed CPO in these layers may be explained in different ways:

1. The graphite-rich layers were deformed by dislocation flow processes and developed a CPO, but this fabric was destroyed during subsequent static recrystallisation. This is unlikely as it would beg the question why the CPO was not destroyed in the graphite-free layers. Also, static recrystallisation appears not to be very effective in destroying a CPO (e.g. Rutter et al., 1994).

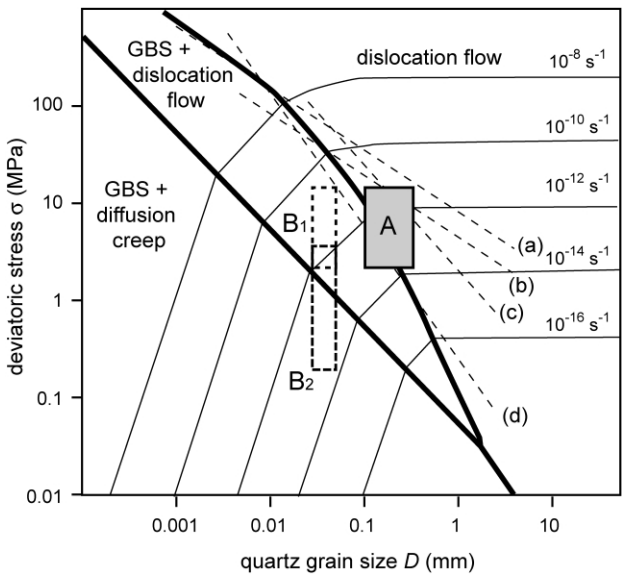

Fig. 9. Deformation mechanism map, with special application to grain boundary sliding of quartz (solid lines; after Etheridge and Wilkie, 1979). Superimposed (dashed lines) are dynamic recrystallised grain size: (a) is after Twiss (1977), (b) after Mercier et al. (1977), (c) and (d) after Christie et al. (1980). Box A indicates approximate conditions of deformation of the graphite-free layers, box B1 indicates approximate conditions of deformation the graphitic layers assuming equal deviatoric stress; box B2 assuming equal strain rate. GBS = grain boundary sliding; DF = dislocation flow.

2. The graphite-rich layers did not deform sufficiently to develop a CPO. Given the strong mylonitic fabric and the parallelism with the graphite-free layers with their strongly developed CPO this is also unlikely.
3. The graphite-rich layers were deformed by a mechanism that does not produce CPO (such as diffusion creep or solution–precipitation creep) combined with a mechanism that actively destroys CPO, such as grain boundary sliding. There is local evidence for dislocation creep within graphite-rich layers; that would be expected to produce some CPO. This suggests that processes were active by which CPO is destroyed. Direct, unequivocal evidence of grain boundary sliding in naturally deformed rocks is difficult to obtain (compare for instance Fliervoet and White (1995) with Fliervoet et al. (1997)). Potential indicators of grain boundary sliding include small grain size, equant grain shape, tabular or diamond grain shape (depending on strain vorticity), grain boundary voids and weak or absent CPO (Boullier and Gueguen, 1975; White, 1977; Behrman, 1986; Behrman and Mainprice, 1987; Drury and Humphreys, 1988; Stünitz and Fitz Gerald, 1993; Ree, 1994). The observations of weak to absent CPO, together with the evidence of large strains at high temperatures, a relatively fine grain size and equant grains support the suggestion that grain boundary sliding was an important flow mechanism in the fine-grained, graphite-rich layers. The progressive weakening of CPO with decreasing grain size suggests that grain boundary sliding became progressively more dominant at the expense of dislocation flow.

Etheridge and Wilkie (1979) have already suggested that second phase particles might be very effective in keeping the quartz grain size within the grain size sensitive field (see Fig. 9). The observations presented in this paper strongly support this suggestion. Their objection to their own suggestion, namely that fabrics in fine-grained mylonites are commonly even stronger than in coarse-grained mylonites, does not apply to the investigated Naxos mylonites.

In a similar study on high-pressure, low-temperature Quartzite–Phyllonite Unit on Crete, Stöckhert et al. (1999) found progressive weakening of quartz CPO with increasing mica content. On the basis of truncated clastic quartz grains and quartz filled pressure shadows, solution precipitation creep was interpreted as the main deformation mechanism in the phyllonites. The differences with the graphitic quartz mylonites from Naxos are that the Quartzite–Phyllonite Unit (see Schwarz and Stöckhert, 1996; Stöckhert et al., 1999): (i) deformed at lower temperatures ($T \sim 400$ °C); (ii) experienced its first metamorphic cycle and presumably still contained ample fluid during deformation, whereas in Naxos significant dehydration presumably took place during M1; (iii) there is positive evidence for solution precipitation creep in the phyllonites; (iv) grain size of quartz clasts in the phyllonite is much coarser (up to 0.4 mm) than in the graphite-rich layers from Naxos; and (v) quartz clasts are still visible in both the quartzite and the phyllonite, possibly indicating that strain was less than in Naxos.

6.3. Accommodation mechanisms for grain boundary sliding

Grain boundary sliding generally must be accompanied by some other accommodating deformation mechanism to solve volume problems around triple junctions during neighbour-switching of grains (e.g. Ashby and Verall, 1973). In small graphite-free areas within the graphite-rich layers, dislocation flow appears to have taken place and is thus one possible accommodation mechanism. Given the high temperature of deformation (500–650 °C), diffusion creep is another possible accommodation mechanism. Since diffusion creep is also grain size sensitive it is likely that with decreasing grain size it became an increasingly more important accommodating mechanism, at the expense of dislocation flow. The degree by which this process was aided by the presence of a metamorphic fluid (solution–precipitation creep) is unclear.

Another accommodation mechanism may be provided by the deformation of graphite. In experiments with octachloropropane, Ree (1994) observed a steady state ratio of 1–3% (vol.) grain boundary voids during deformation. Graphite is likely to be a much weaker phase than quartz. If graphite could easily flow along quartz grain boundaries from one

triple junction to another, it could easily fill the quartz voids and thus provide a significant contribution to the required accommodation strain.

6.4. Grain size, grain size reduction and grain boundary sliding

If grain boundary sliding in quartz was indeed the dominant deformation mechanism in the graphite-rich layers, it occurred at a grain size that is much coarser (~50 μm) than normally reported. In previously reported instances of grain boundary sliding in natural rocks, the grain size is between 5 and 25 μm (Boullier and Gueguen, 1975; Behrman and Mainprice, 1987; Fliervoet et al., 1997). This disparity is partially explained by the relative high temperature and low stress at which the Naxos mylonites were deformed. The dynamically recrystallised quartz grain size in our samples is between 100 and 300 μm, suggesting deviatoric stresses lower than 10 MPa (Fig. 9). The dynamically recrystallised quartz grain size in the study of Fliervoet et al. (1997) for instance is 30–60 μm, suggesting stresses higher than 10 MPa.

According to deformation mechanism maps (Gifkins, 1977; Etheridge and Wilkie, 1979), grain boundary sliding dominated deformation is possible at low stresses with relative coarse grain size (Fig. 9). De Bresser et al. (1998) recently argued that the steady state grain size in a deforming rock has the tendency to settle at the transition from dislocation flow dominated to grain boundary sliding dominated deformation. This would imply that the grain size in a deforming rock only needs to be kept just under the recrystallised 'equilibrium' grain size to favour grain boundary sliding. This implies that a small grain size alone is not a sufficient basis to either suggest or reject grain boundary sliding.

Etheridge and Wilkie (1979) argued that a switch to grain-size sensitive deformation solely driven by grain size reduction by dynamic recrystallisation is unlikely for pure quartz. For different reasons, De Bresser et al. (1998) arrived at the same conclusion. This study supports that assertion in that grain boundary sliding was only dominant where grain boundaries were pinned by a second phase. Other instances of reported grain boundary sliding are in polymineralic rocks such as quartzo-feldspathic ultramylonite (Behrman and Mainprice, 1987; Fliervoet et al., 1997) or peridotite (Boullier and Gueguen, 1975). It thus appears that grain boundary sliding is unlikely in pure quartzite mylonites, but may be a normal occurrence in impure quartzite, quartzo-feldspathic mylonite or other polymineralic rocks.

7. Conclusions

1. In high grade quartz mylonites of Naxos, Greece, dispersed graphite particles effectively inhibited grain boundary migration and grain growth of quartz, provided the graphite particles have a minimum diameter of about 5 μm. Inhibition of grain boundary migration resulted in a stabilised quartz grain size below the dynamic recrystallisation grain size. The stabilised quartz grain size is inversely dependent on the degree of dispersion.
2. Due to quartz grain size stabilisation, deformation in the graphite-rich layers was dominated by grain boundary sliding, whereas deformation in the graphite-free layers was dominated by dislocation flow. Progressive weakening of CPO concomitant with progressive increase in dispersion and decrease in quartz grain size suggest that the deformation mechanism switch from dislocation flow to grain boundary sliding was gradual.
3. In the Naxos quartz mylonites, different deformation mechanisms operated in very close proximity, under the same pressure and temperature conditions, with grain size and deformation mechanism primarily controlled by the presence of a dispersed second phase. Grain boundary sliding of quartz occurred at relatively coarse grain size, compared with other reported instances of grain boundary sliding. These observations emphasise the importance of a dispersed second phase on the rheological behaviour of rocks.

Acknowledgements

Paul Bons, Reinoud Vissers, Jeroen Krabbendam and Hans de Bresser are thanked for assistance with various analytical techniques. Gordon Lister and Mark Jessel are thanked for commenting on an early version of the manuscript. Toru Takeshita and Bernhard Stöckhert are thanked for reviews which much improved the manuscript.

Appendix A. Estimating the volume fraction of a second phase from transmitted light images of thick sections

Assume a sample dispersed with opaque convex particles in a transparent matrix. From stereology we know that the expected volume fraction V_V of particles is equal to the expected area fraction A_A in randomly selected 2-D cross-sections, the expected length fraction L_L in randomly selected 1-D cross-sections and the expected point fraction P_P for points on an arbitrary grid:

$$V_V = A_A = L_L = P_P \tag{A1}$$

Here we focus on estimation of the volume fraction from measurements of the area fraction in projections through slices of finite thickness, t. Projections through 'thick' sections show a larger area of the opaque phase than a 2-D cross-section. It is clear that the bias in volume fraction depends on the size of the particles and the thickness of the slice. We briefly review existing techniques and then

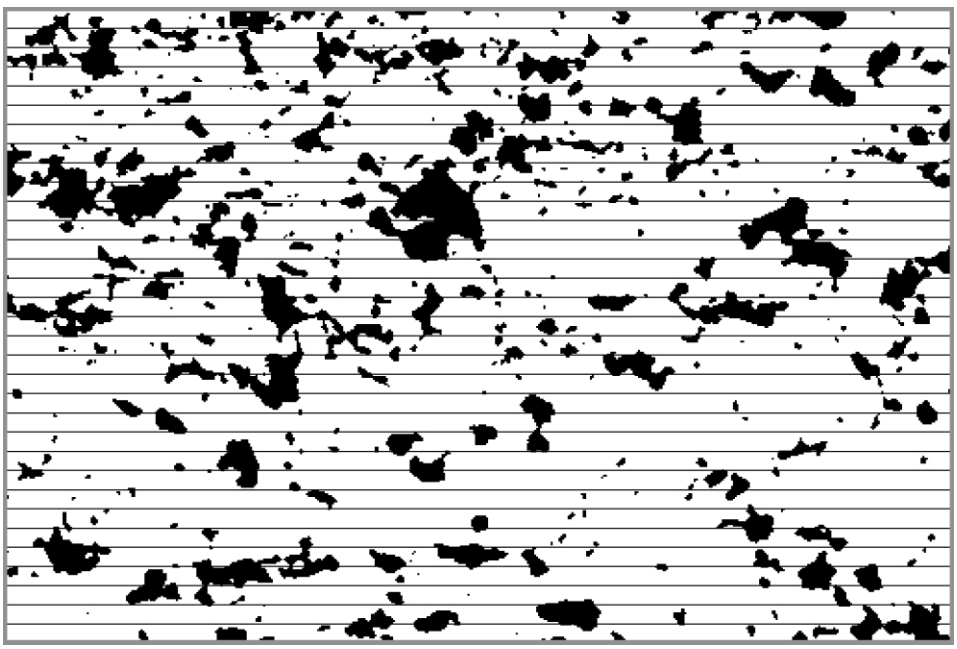

Fig. A1. Segmented binary image of a micrograph of a graphitic quartzite, plane polarized light. The lines superimposed on the image indicate strips whose width is equal to the section thickness. See text for discussion.

present a new method to correct for this phenomenon. Earlier models are suitable only for very thin sections in which the slice thickness is much smaller than the object diameter. The method presented here can be applied to thicker sections as well.

Cahn and Nutting (1959) presented an unbiased estimator of the true area fraction A_A of the opaque phase based on the observed area fraction A'_A from thin slices:

$$A_A = A'_A - \frac{t}{4} S_V \tag{A2}$$

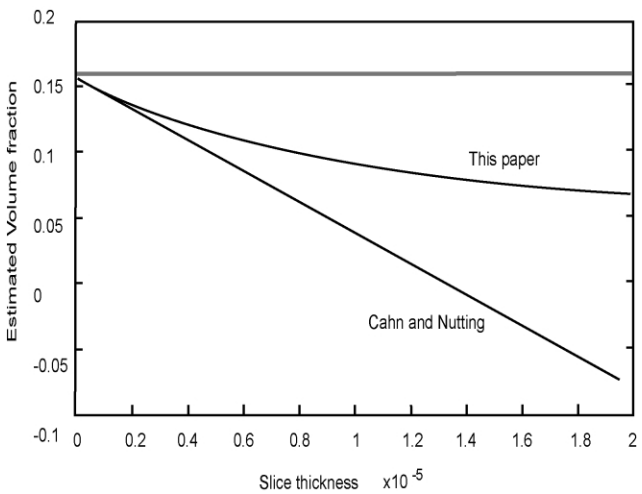

Fig. A2. Diagram showing estimated volume fraction of graphite as a function of section thickness, as calculated for the same image by the two methods discussed in the text. Thick horizontal line represents the area fraction observed in the image. Note that the method of Cahn and Nutting (1959) yields unrealistic values at large thickness, but also that the two methods converge at very small section thickness.

with S_V the amount of surface per unit volume and t the slice thickness. This correction is only valid for particles with diameter R such that $t \ll R$.

The surface density S_V has dimension length^{-1}. This suggests that we may estimate S_V indirectly through the boundary length per unit area, B_A, or the number of boundary intersections per unit length, P_L. This can be done writing the relationship between S_V, B_A, and P_L:

$$S_V = \frac{4}{\pi} B_A = 2P_L \tag{A3}$$

Using B_A to compute S_V requires a suitable algorithm for computing the perimeter of objects in digitized images (Vossepoel and Smeulders, 1982; Young, 1988).

For relatively thick slices, the correction proposed by Cahn and Nutting (1959) does not hold, because the slice thickness does not fulfil the condition that it is small compared with the object diameter. Under these circumstances we can apply a different approach.

The projected area of an opaque object in a thick section of thickness t is now substantially larger than the area of the object in the top-surface of the thick section. Using an empirical method we can estimate the increase in observed area. It assumes that the objects in the projected image have shapes, sizes and total fill-factor that is comparable with an infinitely thin cross-section through the original volume. If so, we can apply the projection to non-overlapping strips in the two-dimensional images and measure the increase in length-fraction compared with the original area-fraction. The width of these strips must be equal to the thickness of the original slice. The ratio between the observed area- and length-fractions can be used to compensate for the increase

in observed area-fraction:

$$V_V = \frac{A'_A}{L''_L} A'_A \quad \text{(A4)}$$

with A'_A the observed area-fraction in the thick slice, and L''_L the observed length-fraction using a projection through a thick strip. For thin slices this method and the correction by Cahn and Nutting (1959) should converge to the same value.

To illustrate the method we apply it to the segmented binary image shown in Fig. A1. The image contains 2040 × 1360 pixels. The lateral sampling pitch is 0.45 μmm, which corresponds to an image size of 0.92 mm × 0.613 mm. The slice thickness is 0.2 mm. The horizontal lines superimposed on the image indicate the strips whose width is equal to the thickness of the slice. Note that the slice thickness is large compared with the object diameter.

In Fig. A2 we plotted the estimated volume fraction based on the two methods presented as a function of slice thickness. The two correction methods are identical for small slice thicknesses, as expected. For medium and large slice thickness the method by Cahn and Nutting fails and may even yield negative volume fractions. The new method in this paper behaves as expected.

References

Andriessen, P.A.M., Boelrijk, N.A.I.M., Hebeda, E.H., Priem, H.N.A., Verdurmen, E.A.T., Verschure, R.H., 1979. Dating the events of metamorphism and granitic magmatism in the Alpine Orogen of Naxos (Cyclades, Greece). Contributions to Mineralogy and Petrology 69, 215–225.

Ashby, M.F., Centramore, M.A., 1968. The dragging of small oxide particles by migrating grain boundaries in copper. Acta Metallurgica 19, 1081–1092.

Ashby, M.F., Verall, R.A., 1973. Diffusion-accommodated flow and superplasticity. Acta Metallurgia 21, 149–163.

Avigad, D., 1998. High-pressure metamorphism and cooling on SE Naxos (Cyclades, Greece). European Journal of Mineralogy 10, 1309–1319.

Behrman, J.H., 1986. Crystal plasticity and superplasticity in quartzite; a natural example. Tectonophysics 115, 101–129.

Behrman, J.H., Mainprice, D., 1987. Deformation mechanisms in a high-temperature quartz-feldspar mylonite: evidence for superplastic flow in the lower continental crust. Tectonophysics 140, 297–305.

Boullier, A.M., Gueguen, Y., 1975. SP-mylonites: origin of some mylonites by superplastic flow. Contributions to Mineralogy and Petrology 50, 93–104.

Buick, I.S., 1991. Mylonite fabric development on Naxos, Greece. Journal of Structural Geology 13, 643–655.

Buick, I.S., Holland, T.J.B., 1989. The P–T–t path associated with crustal extension, Naxos, Cyclades, Greece. In: Daly, J.S., Cliff, R.A., Yardley, B.W.D. (Eds.), Evolution of Metamorphic Belts. Geological Society Special Publications 43, pp. 365–369.

Cahn, J.W., Nutting, J.W., 1959. Transmission quantitative microscopy. Trans. AIME 215, 526.

Christie, J.M., Ord, A., Koch, P.S., 1980. Relationship between recrystallized grain size and flow stress in experimentally deformed quartzite. Eos, Transactions American Geophysical Union 61, 377.

De Bresser, J.H.P., Peach, C.J., Reijs, J.P.J., Spiers, C.J., 1998. On dynamic recrystallization during solid state flow; effects of stress and temperature. Geophysical Research Letters 25, 3457–3460.

Drury, M.R., Humphreys, F.J., 1988. Microstructural shear criteria associated with grain-boundary sliding during ductile deformation. Journal of Structural Geology 10, 83–89.

Drury, M.R., Urai, J.L., 1990. Deformation-related recrystallization processes. Tectonophysics 172, 235–253.

Etheridge, M.A., Wilkie, J.C., 1979. Grainsize reduction, grain boundary sliding and the flow strength of mylonites. Tectonophysics 58, 159–178.

Evans, B., Renner, J., Hirth, G., 2001. A few remarks on the kinetics of static grain growth in rocks. International Journal of Earth Sciences (Geologische Rundschau) 90, 88–103.

Fliervoet, T.F., White, S.H., 1995. Quartz deformation in a very fine grained quartzo-feldspathic mylonite; a lack of evidence for dominant grain boundary sliding deformation. Journal of Structural Geology 17, 1095–1109.

Fliervoet, T.F., White, S.H., Drury, M.R., 1997. Evidence for dominant grain-boundary sliding deformation in greenschist- and amphibolite-grade polymineralic ultramylonites from the Redbank deformed zone, central Australia. Journal of Structural Geology 19, 1495–1520.

Gifkins, R.C., 1977. The effect of grain size and stress upon grain-boundary sliding. Metallurgical Transactions 8, 1507–1516.

Herwegh, M., Jenni, A., 2001. Granular flow in polymineralic rocks bearing sheet silicates: new evidence from natural examples. Tectonophysics 332, 309–320.

Humphreys, F.J., Hatherly, M., 1996. Recrystallization and Related Annealing Phenomena, Elsevier, Amsterdam.

Jansen, J.B.H., Schuiling, R.D., 1976. Metamorphism on Naxos; petrology and geothermal gradients. American Journal of Science 276, 1225–1253.

Kreulen, R., 1977. CO2-rich fluids during regional metamorphism on Naxos, a study on fluid inclusions and stable isotopes. PhD thesis, University of Utrecht.

Law, R.D., 1990. Crystallographic fabrics: a selective review of their applications to research in structural geology. In: Knipe, R.J., Rutter, E.H. (Eds.), Deformation mechanisms, rheology and tectonics. Geological Society Special Publication 54, 335–352.

Lister, G.S., Banga, G., Feenstra, A., 1984. Metamorphic core complexes of Cordilleran type in the Cyclades, Aegean Sea, Greece. Geology 12, 221–225.

Mercier, J.C., Anderson, D.A., Carter, N.L., 1977. Stress in the lithosphere; inferences from steady state flow of rocks. Pure and Applied Geophysics 115, 119–226.

Olgaard, D.L., 1990. The role of second phase in localizing deformation. In: Knipe, R.J., Rutter, E.H. (Eds.), Deformation Mechanisms, Rheology and Tectonics. Geological Society Special Publication 54, pp. 175–181.

Olgaard, D.L., Evans, B., 1986. Effect of second-phase particles on grain growth in calcite. Journal of the American Ceramics Society 69, 272–277.

Olgaard, D.L., Evans, B., 1988. Grain growth in synthetic marbles with added mica and water. Contributions to Mineralogy and Petrology 100, 246–260.

Passchier, C.W., Trouw, R.A.J., 1996. Microtectonics. Springer, Berlin. 289 pp.

Ree, J.H., 1994. Grain boundary sliding and development of grain boundary openings in experimentally deformed octachloropropane. Journal of Structural Geology 16, 403–418.

Rutter, E.H., Casey, M., Burlini, L., 1994. Preferred crystallographic orientation development during the plastic and superplastic flow of calcite rocks. Journal of Structural Geology 16, 1431–1446.

Schmid, S.M., 1982. Microfabric studies as indicators of deformation mechanisms and flow laws operative in mountain building. In: Hsu, K.J., (Ed.), Mountain Building Processes, Academic Press, London, pp. 95–110.

Schwarz, S., Stöckhert, B., 1996. Pressure solution in siliciclastic HP–LT

metamorphic rocks; constraints on the state of stress in deep levels of accretionary complexes. Tectonophysics 255, 203–209.

Stöckhert, B., Wachmann, M., Kuester, M., Bimmermann, S., 1999. Low effective viscosity during high pressure metamorphism due to dissolution precipitation creep; the record of HP–LT metamorphic carbonates and siliciclastic rocks from Crete. Tectonophysics 303, 299–319.

Stünitz, H., Fitz Gerald, J.D., 1993. Deformation of granitoids at low metamorphic grade. II. Granular flow in albite-rich mylonites. Tectonophysics 221, 299–324.

Stüwe, H.P., 1978. Driving forces and dragging forces in recrystallization. In: Haessner, F. (Ed.), Recrystallization of Metallic Materials, pp. 11–21. Dr Rieder Verlag, Stuttgart.

Takeshita, T., 1996. Estimate of the physical conditions for deformation based on *c*-axis fabric transitions in naturally deformed quartzite. The Journal of the Geological Society of Japan 102, 211–222 (in Japanese with English Abstracts)..

Tullis, J., Christie, J.M., Griggs, D.T., 1973. Microstructures and preferred orientations of experimentally deformed quartzites. Geological Society of America Bulletin 84, 297–314.

Twiss, R.J., 1977. Theory and applicability of a recrystallized grain size palaeopiezometer. Pure and Applied Geophysics 115, 227–244.

Urai, J.L., Feenstra, A., 2001. Weakening associated with the diaspore-corundum dehydration reaction in metabauxites: an example from Naxos (Greece). Journal of Structural Geology 23, 941–950.

Urai, J.L., Jessell, M., 2001. Recrystallization and grain growth in minerals: recent developments. In: Gottstein, G., Molodov, D. (Eds.), Recrystallization and Grain Growth, Proceedings of the first Joint International Conference, August 27–31 2001, RWTH Aachen, Germany. Springer Verlag, Berlin, pp. 87–96.

Urai, J.L., Means, W.D., Lister, G.S., 1986. Dynamic recrystallization of minerals. American Geophysical Union, Geophysical Monograph 36, 161–199.

Urai, J.L., Schuiling, R.D., Jansen, J.B.H., 1990. Alpine deformation on Naxos. In: Knipe, R.J., Rutter, E.H. (Eds.), Deformation Mechanisms, Rheology and Tectonics. Geological Society Special Publications 54, pp. 509–522.

Vossepoel, A.M., Smeulders, A.W.M., 1982. Vector code probabilities and metrication error in the representation of straight lines of finite length. Computer Graphics and Image Processing 20, 347–364.

White, S., 1977. Geological significance of recovery and recrystallization processes in quartz. Tectonophysics 39, 143–170.

White, S.H., Burrows, S.E., Carreras, J., Shaw, N.D., Humphreys, F.J., 1980. On mylonites in ductile shear zones. Journal of Structural Geology 2, 175–187.

Wijbrans, J.R., McDougall, I., 1988. Metamorphic evolution of the Attic Cycladic metamorphic belt on Naxos (Cyclades, Greece) utilizing $^{40}Ar/^{39}Ar$ age spectrum measurements. Journal of Metamorphic Geology 6, 571–594.

Young, I.T., 1988. Sampling density and quantitative microscopy. Analytical and Quantitative Cytology and Histology 10 (4), 269–275.